A 3D Sliding Mode Control Approach for Position Based Visual Servoing System

Mahsa Parsapour, Soheil RayatDoost, and Hamid D. Taghirad,

Advanced Robotics and Automated Systems (ARAS), Industrial Control Center of Excellence (ICEE),
Faculty of Electrical and Computer Engineering, K. N. Toosi University of Technology, Tehran, Iran
E-mail: mahsa.parsapour.1989@ieee.org , s.rayatdoost@ut.ac.ir , taghirad@kntu.ac.ir
Phone: + 98 21 8846 9084
Fax: + 98 21 8846 2066
Postal Address: Seyedkhandan, Dr. Shariati Ave,Tehran, Islamic Republic of Iran. P.O BOX: 16315-1355

Abstract

The performance of visual servoing systems can be enhanced through nonlinear controllers. In this paper, a sliding mode control is employed for such purpose. The controller design is based on the outputs of a pose estimator which is implemented on the scheme of the position-based visual servoing (PBVS) approach. Accordingly, a robust estimator based on unscented Kalman observer cascading with Kalman filter is used to estimate the position, velocity and acceleration of the target. Therefore, a PD-type sliding surface is selected as a suitable manifold. The combination of the estimator and nonlinear controller provides a robust and stable structure in PBVS approach. The stability analysis is verified through Lyapunov theory. The performance of the proposed algorithm is verified experimentally through an industrial visual servoing system.

Keywords: Nonlinear controller, Position-based visual servoing, Unscented Kalman filter, PD-type sliding surface, Lyapunov theory.

I.   INTRODUCTION

Visual servoing (VS) is applied for tracking the movement of any specific objects based on a vision input. Different research fields, like robotics, image processing, and control are applied to achieve VS. It has wide applications in robotics and Mechatronic systems like medical robotics, planetary robotics and especially their extensive application in industrial robots, [1], [2]. The respective control loop in VS has different architectures such as look-and-move structure and per Weiss structure [3]. Look-and-move structure has an internal feedback controller, as being used in many industrial robots. Such setups may accept Cartesian velocity or incremental position commands and permits to simplify the design of control signal [3].

There are three main approaches in VS [4], position based visual servoing (PBVS) [5], image based visual servoing (IBVS) [6], and "2&1/2 D" visual servoing [7], where PVBS is the most frequently used methods [5]. In PBVS, the control signal is produced based on the estimation of position and orientation (pose) of the target with respect to the camera. The accuracy of the estimated pose is directly related to the measurement noise and the camera calibration [8]. Extended Kalman filter (EKF) and Unscented Kalman filter (UKF) has been developed to deal with the pose estimation in the noisy and uncertain situations. The aforementioned estimators have shown to be quite effective in practice [9,10,11]. In order to include the velocity and acceleration of the target, the appropriate dynamic model for the relative motion between the camera and the target is necessary. Conventional models are applied based on the constant velocity or the acceleration model which assumes invariable relative velocity or acceleration at each sample time [1].

After estimating the pose of the target object, the main goal in VS problem is to enhance the performance of tracking via a controller. Since the system in hand (a robot) has nonlinear dynamics, a nonlinear controller has to be designed for this purpose. For such a design, we use sliding mode control (SMC) in order to achieve the robust performance in the noisy environment as in the industrial environments. Generally, in many forms of VS the path planning and controlling the end effector of robot are performed separately. By using SMC approach, the aforementioned tasks can be combined together. The combination helps to tune the whole control system together. In SMC, all states of the system are enforced to converge toward a desired sliding surface within a finite time and to stay on this manifold for all further times. In present paper, we define a PD-type sliding mode surface to generate a desired path. The novelty of such selection is the employment of the estimated position, velocity and acceleration of the target for defining the sliding manifold. The estimated values are obtained from a UKF cascade structure that authors recently proposed in [11]. The information of the estimated model and the observation inherits uncertainties, which can be directly considered in the proposed controller. The stability of the closed-loop system is proved by Lyapunov theory. As the target object is dynamically changing (in contrast to the pre-planned path), the sliding surface is adapted to the varying positions in the present case.

So far, various types of SMC have been used for VS system in [12,13,14]. Usually, based on the nonlinear dynamics model of the system, SMC is designed. To the best knowledge of the

authors, the stability analysis of the closed-loop system with the combination of the pose estimator in the uncertain and noisy situations has not been focused significantly. SMC for PBVS problem has been introduced theoretically for a 6 DOF robot manipulator in [15]. The desired path is defined in which errors are bounded, and the target visibility is guaranteed. In [16], a sliding surface is designed with the consideration of uncertainties in the nonlinear dynamics of the robot. The proposed algorithm in [16], used dynamics of robot that is too complex to implement on industrial robots. In our case, PD-type sliding surface is developed for a five degrees of freedom robot manipulator, with PBVS approach. The existence of the internal feedback controller on the industrial robot manipulator makes the controller design simpler, since the robot accepts the position command in the task space. Through the internal loop, a simplified motion kinematics model can be used for the industrial robot, where the controller inputs are the joint velocity signal. To produce the control signal, the information of the pose estimator is used as the sliding manifold's input. Finally, the tracking performance of the adapted control scheme on the industrial robot is verified experimentally.

II. THEORETICAL BACKGROUND

In this section, first experimental setup that has been used for VS purpose is presented. Then, the formulation of UKO+KF pose estimators is reviewed. Furthermore, practical implementation issues of applying control outputs to an industrial manipulator are described.

A. Experimental Setup

The experimental hardware setup, which is shown in Fig. 1, consists of a 5-DOF RV-2AJ robot manipulator produced by Mitsubishi Co. augmented with a one degree of freedom linear gantry. This robot has five degrees of freedom motion, with one degree of redundancy, but the orientation of the wrist about the tool axis is not presented in the structure. Additionally a PC equipped with a Pentium IV (1.84 GHz) processor and a 1 GB of RAM is utilized as the processor. A camera is attached on the end effector of the manipulator, which is a Unibrain Co. product with 30fs frame rate and a wide lens with 2.1 mm focal length. Since we need a real-time setup, OPENCV Library is used in the Visual Studio environment.

B. Feature Extraction and Pose Estimation

In the conventional pose estimation, the relative pose of the object with respect to the camera frame in 3D coordinates is calculated. To perform this calculation, some specified points as feature points attached to the target object in 2D coordinates of the image are needed. In Fig. 2, the projections of feature points are illustrated in the image frame which denoted by $p_i^{im} = (u_i, v_i)$; $i = 1, \ldots, n$. The feature points in the object frame can be expressed as $p_i^o = (x_i^o, y_i^o, z_i^o)$; $i = 1, 2, \ldots, n$, $n \geq 3$; and represented in the camera frame by $p_i^c = (x_i^c, y_i^c, z_i^c)$. The relationship between p_i^c and p_i^o can be defined as the following equation

$$p_i^c = R(roll, pitch, yaw).p_i^o + T \tag{1}$$

in which, roll, pitch and yaw are the orientation Euler angles and the translation are represented by vector $T = [X \, Y \, Z]^T$.
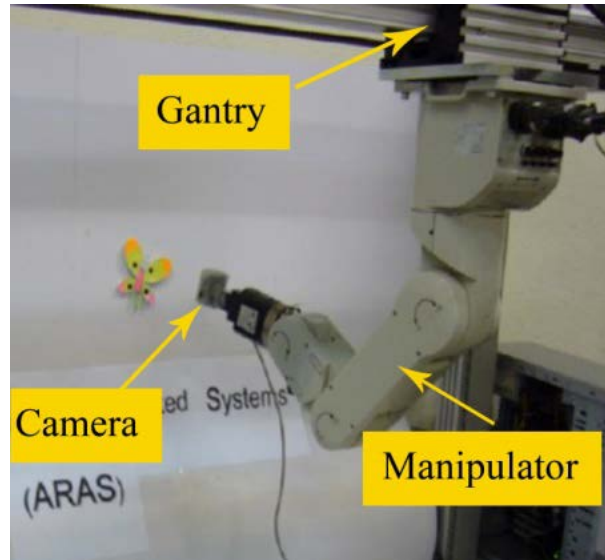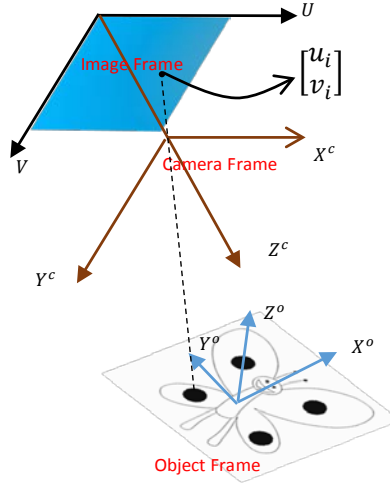

Fig. 1: Experimental setup

Fig. 2: Camera, object and image frames

Using a pin-hole camera model, the relationship between p_i^{im} and p_i^c can be formulated as follows

$$\begin{bmatrix} u_i \\ v_i \end{bmatrix} = \begin{bmatrix} -\dfrac{f}{P_x} & -\dfrac{f}{P_y} \end{bmatrix} \cdot \begin{bmatrix} \dfrac{x_i^c}{z_i^c} \\ \dfrac{y_i^c}{z_i^c} \end{bmatrix} \tag{2}$$

In this equation, f is the focal length and P_x, P_y are inter-pixel spacing parameters along u_i and v_i. By folding the 3n equations (1) into the camera model (2), a set of 2n nonlinear equations is achieved. In order to solve this set of nonlinear equations and achieve a unique solution, at least 3 non-aligned points on the object are required [17]. There are several researches that apply EKF and UKF for pose estimation [18, 19]. Recently, [9] proposed EKF in addition to KF that guarantees its convergence; however, in [11] it is shown that the performance of this method is directly dependent to the initial condition, and therefore, the employment of UKF instead of EKF leads to better performance. Due to the promising features of this estimator, this technique is used as the pose estimator engine in this paper. In this estimator, the nonlinear-uncertain estimation problem is decomposed into a nonlinear-certain observation in addition to a linear-uncertain estimation problem. The first part is handled using the unscented Kalman observer (UKO) and the second part is accomplished by a Kalman filter (KF). The pose estimator is fed to a robust and fast modified principal component analysis (PCA) based feature extractor proposed in [11]. This robust method is used in this article to estimate the target pose in an uncertain and noisy environment.

C. Singularity Avoidance

After estimating the desired dynamic parameter of target, these parameters have to be converted to the joint space of the robot manipulator. Since there is no prior knowledge on the desired trajectory, and the robot is a five degrees-of-freedom manipulator, it may encounter singular configurations within its prescribed trajectory. To remedy this issue, inverse kinematic of the manipulator is solved in a real-time routine to generate a singular free motion with the consideration of the joint limits for the robot. A practical motion planner which is proposed by the authors in [20] is fully elaborated. The applied method shows a well performance, when there is no prior information about the via-points and the final destination of the desired trajectory.

Fig. 3 represents the complete loop of the visual servoing system. An image is captured by the camera applied as the input of the "Feature Extractor" block. After estimating the target pose by UKO+KF, the relative pose is commanded to the SMC as a desired position.
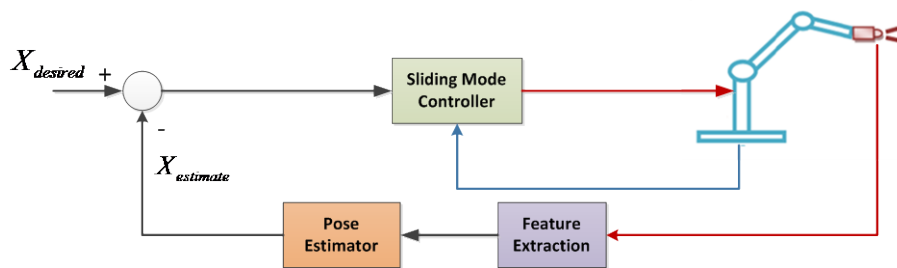

Fig. 3: The complete VS loop

III.   DESIGN OF SMC FOR PBVS SYSTEM

The whole process of the VS loop is demonstrated in Fig. 4. In the first step, an image is captured by a camera. Then the desired features are extracted from the mentioned image. After that the position, velocity and acceleration of the object are estimated by UKO+KF estimator. Error which is defined as the relative pose is applied as the input to the sliding surface. Then control signal (in velocity level) is produced via SMC, which is proportional to each degree-of-freedom (DOF) of the robot. According to singularity avoidance, such signals are employed to solve the inverse kinematics problem in order to calculate the angle of each joint. In final step, the outcome signal is commanded the internal controller of our industrial robot. Note that, because of the internal controller, we can assume the controller as a prefect tracker. The whole process is repeated until the target object is tracked perfectly.
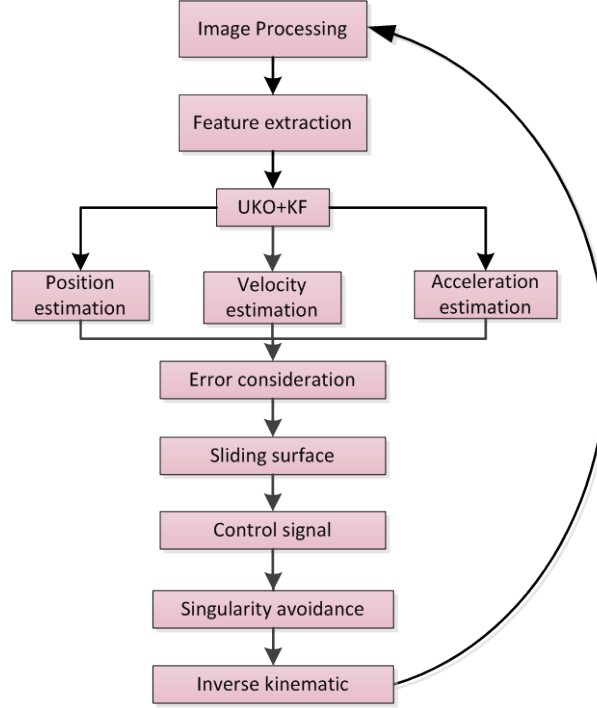
Fig. 4: Block diagram of the overall process

Traditionally, a visual servoing system includes the feature tracking and the feedback controlling as two separate processes. This separation limits tuning of the whole system performance. In present paper, we propose to use SMC to perform VS for mentioned tasks. The path planning is accomplished using the sliding mode surface, and the performance is preserved by the sliding mode control output. The stability of the whole control system is proved by Lyapunov theory. Moreover, the robust behavior of SMC against the estimation noise provides a suitable tracking performance for the whole visual servoing systems.

A. Controller Design

In this approach, instead of using the dynamics of the system, we have used the estimated values from UKO+KF and their corresponding desired values to define the sliding mode surface. The main purpose is tracking a specific object, whether the object is moving or not. According to section II-A, by substituting the equations (1) into the pin-hole camera model (2), a set of nonlinear equations is obtained as (3). These nonlinear equations show the relation between "the relative pose of the target object with respect to the end-effector (camera) frame in the 3D coordinates" and "the feature points attached to the target object in 2D coordinate of the image frame".

$$G\left(X,Y,Z,roll,pitch,yaw\right)=\begin{bmatrix}u_i\\v_i\end{bmatrix}, \qquad\qquad i=1,2,\ldots,n\,,\ \ n\geq3 \tag{3}$$

$$=\begin{bmatrix}-\dfrac{f}{P_x}*\dfrac{X+\cos\left(roll\right)\cos\left(pitch\right)x_i^o+\left(\cos\left(roll\right)\sin\left(pitch\right)\sin\left(yaw\right)-\sin\left(roll\right)\cos\left(yaw\right)\right)y_i^o+\left(\cos\left(roll\right)\sin\left(pitch\right)\cos\left(yaw\right)+\sin\left(roll\right)\sin\left(yaw\right)\right)z_i^o}{Z-\sin\left(pitch\right)x_i^o+\cos\left(pitch\right)\sin\left(yaw\right)y_i^o+\cos\left(roll\right)\cos\left(yaw\right)z_i^o}\\[4mm]-\dfrac{f}{P_y}*\dfrac{Y+\sin\left(roll\right)\cos\left(pitch\right)x_i^o+\left(\sin\left(roll\right)\sin\left(pitch\right)\sin\left(yaw\right)+\cos\left(roll\right)\cos\left(yaw\right)\right)y_i^o+\left(\sin\left(roll\right)\sin\left(pitch\right)\sin\left(yaw\right)-\cos\left(roll\right)\sin\left(yaw\right)\right)z_i^o}{Z-\sin\left(pitch\right)x_i^o+\cos\left(pitch\right)\sin\left(yaw\right)y_i^o+\cos\left(roll\right)\cos\left(yaw\right)z_i^o}\end{bmatrix}$$

By considering a constant velocity model that assumes invariable relative velocity of the target object with respect to the end-effector at each sample time, we may reach the following model for the relative pose of the object with respect to the end-effector:

$$\begin{aligned}W_k &= AW_{k-1}+\mu_k\\P_k &= G\left(W_K\right)+\delta_k\end{aligned} \tag{4}$$

where $W=\left[X,\ \dot{X},Y,\ \dot{Y},Z,\ \dot{Z},roll,\ \dot{roll},pitch,\ \dot{pitch},yaw,\ \dot{yaw}\right]^T$, and A is a block diagonal matrix with $\begin{bmatrix}1 & T\\0 & 1\end{bmatrix}$ blocks. μ_k and δ_k are the model uncertainty and the measurement noise, respectively, and they are expressed by a zero mean Gaussian noise. P_k is a vector of the normalized coordinates of the feature points in the image plane.

u_i and v_i (for at least 3 non-aligned feature points which are attached to the target object) are calculated by Eq. (2). These points are fed into a UKO to estimate the vector W. The estimation process is explained in [21]. According to the proposed structure in [9, 11], the pose vector is estimated by UKO in an iterative loop with the desired stop condition. Here, the estimated velocity is zero, since the same input is used in several epochs. Moreover, utilizing only one set of input data causes an inaccurate estimation. To overcome such problem, and to estimate the velocity and acceleration of the object, the UKO output is fed to a linear Kalman filter. Then by changing the output and considering a constant acceleration model that assumes invariable relative acceleration at each sample time, we may reach the following linear model:

$$\begin{aligned}V_k &= BV_{k-1}+v_k\\P_{o_k} &= CV_k+\eta_k\end{aligned} \tag{5}$$

where $V=\left[X,\ \dot{X},\ \ddot{X},\ Y,\ \dot{Y},\ \ddot{Y},\ Z,\ \dot{Z},\ \ddot{Z},roll,\dot{roll},\ddot{roll},pitch,\ \dot{pitch},\ \ddot{pitch},\ yaw,\ \dot{yaw},\ \ddot{yaw}\right]$ the state vector that shows the relative motion parameters between the camera and the target object.

B is a block diagonal matrix with $\begin{bmatrix} 1 & T & 0.5T^2 \\ 0 & 1 & T \\ 0 & 0 & 1 \end{bmatrix}$ blocks. P_{o_k} is the pose vector with 6 translational and rotational elements as X, Y, Z, roll, pitch and yaw. η_k and v_k are the model uncertainty and the measurement noise vectors, respectively. v_k is related to the static pose estimator precision. C is a 6×18 matrix with the following format:

$$c_{ij} = \begin{cases} 1 & j = 4i-3 \\ 0 & otherwise \end{cases} \tag{6}$$

Having the mentioned linear model and the desired accuracy of the initial estimation, the KF method is implemented by the recursive formulation to estimate the pose, velocity and acceleration of the target object with respect to the end-effector. After the estimation process, we can define the desired sliding surface. Let us define the following PD-type sliding surface:

$$S = \left(\frac{d}{dt} + \lambda \right) e = \dot{e} + \lambda e \tag{7}$$

in which, e is the relative pose of estimated position of target with respect to position of the end-effector. And, λ is the positive constant which specifies the rate of convergence toward the sliding mode manifold. The sliding surface vector in (7) is a five tuple $S = \begin{bmatrix} s_x & s_y & s_z & s_A & s_B \end{bmatrix}^T$ which contains the manifold motion variable in x, y, z directions and orientation about the z and y axis of the robot base coordinate, called in here A, and B orientations, respectively. Based on the relative pose, the state vector is converged toward the sliding surface. Then the state shall smoothly slide on the surface to reach the target state. Because of the movement of the target, the trajectory path is dynamically changing. Therefore, the position of the current state may diverge from the sliding surface. Hence, the process has to be executed iteratively with a short refreshing period to adapt to the varying positions. There are two approaches to define the required control signal.

The first control design is proposed as follows:

$$v_{e-e}^1 = -\beta(t)\,sgn(S) \tag{8}$$

in which, $\beta(t)$ is a varying time coefficient which will be discussed in the next section. $sgn(\cdot)$ denotes the signum function.

The second control signal design is proposed as follows:

$$v_{e-e}^2 = -\lambda^{-1}\ddot{e} + v_{des} - ksgn(S)$$ (9)

in which, k is the positive constants. $\ddot{e}$ is the acceleration error between the end-effector and the goal. And, v_{des} is the desired velocity of the object.

The first design consists of only a switching term while in the second design, a linearizing term is added to the switching term to ensure the sliding condition [22].

B. Stability Analysis

In the design of the control laws, the sliding condition of the manifold is equal to $\dot{e} + \lambda e = 0$, that constrains the motion of the system. Choosing $\lambda > 0$ guarantees that all the states of the system tend to zero as time tends to infinity. The rate of the convergence can be controlled by the choice of λ. The following derivative equation is needed to obtain the control signal:

$$\dot{S} = \ddot{e} + \lambda\dot{e} = \ddot{e} + \lambda\left(v_{e-e}^1 - v_{des}\right)$$ (10)

Where $\dot{e}$ represents the difference between the velocity of the end-effector and the target. Furthermore, v_{e-e} is the end effector velocity, which has been used as the control signal in the practical implementation.

The stability analysis of this algorithm is based on Lyapunov direct method. Consider the following positive definite Lyapunov function candidate $V = \dfrac{1}{2}S^T S$. To show the stability of this algorithm, the derivative of the Lyapunov function candidate has to be negative. To provide these circumstances, the control signal has to be limited by a specified function. This function is subject to the robot velocity constraints and the amplitude of the estimation noise. The following inequality can be specified from (8). Function $\varphi(t)$ will satisfy the following inequality [23].

$$\left\|\frac{\ddot{e} - \lambda v_{des}}{\lambda}\right\|_\infty \leq \varphi(t)$$ (11)

Based on the upper bound of the control signal, the derivative of the Lyapunov function candidate $\dot{S}$ is determined by

$$\dot{V} = S\dot{S} = S\left(\ddot{e} - \lambda v_{des}\right) + S\lambda v_{e-e}^1$$ (12)

$$\dot{V} \le \lambda |S| \varphi(t) + \lambda S v_{e-e}^1 \tag{13}$$

By folding the first control signal equation (8) into (12) the following inequality can be obtained for the derivate of Lyapunov function candidate,

$$\dot{V} \le \lambda |S| \varphi(t) + \lambda S \left(-\beta(t) sgn(S) \right) \tag{14}$$

With the consideration of $\beta(t) \ge \varphi(t) + \beta_0$, the derivative of the Lyapunov function will be semi-negative definite (obviously, $\dot{V} = 0$ when $S = 0$).

$$\dot{V} \le -\lambda \beta_0 |S| \tag{15}$$

Therefore, the trajectory reaches the manifold $S = 0$ in the finite time and, once on the manifold, it cannot leave it, as forced by the condition (15).

The same procedure can be done for the second controller design. Combining (9) and (12) we have,

$$\dot{V} = S \left(\ddot{e} - \lambda v_{des} \right) + S \lambda \left(-\lambda^{-1} \ddot{e} + v_{des} - ksgn(S) \right)$$

$$\dot{V} = -k\lambda |S| \tag{16}$$

In this approach, asymptotic stability is verified by (16) because the derivate of the Lyapunov function candidate is negative definite.

There are some factors to select one of the controllers' designs in our practical implementation. The second control design has a linearizing term in contrast to the first control design. The analysis of the second design can be failed owing to the accuracy estimations in observations, in the presence of uncertainties. On the other hand, the first design permits to presume uncertainties in more suitable condition for VS problem. In the first design, $\beta(t)$ is directly determined the control signal limitations, while in the second design the estimated values from UKO+KF affected such a limitation. Moreover, the command of the robot might be greater than the legal bound of the control signal. Therefore, the first control design is selected for the practical implementation.

C.Modified Controller Design

SMC has encountered some limitations in practice, especially the chattering [22]. The most conventional modification used to limit the chattering is the boundary layer approach [22, 23]. To

attenuate chattering, the signum function can be replaced by a high-slope saturation function. The control law is altered as

$$v_{e-e}^{1} = -\beta(t)\, sat\,(s/\varepsilon) \tag{17}$$

where $sat(\cdot)$ is the saturation function and ε is a positive constant. A suitable approximation requires the use of small ε. For the stability analysis, a similar analysis can be performed when $|S| \geq \varepsilon$, and the derivatives of the Lyapunov function satisfies the inequality $\dot{V} \leq -\lambda \beta_0 |S|$. Therefore, whenever $|S| \geq \varepsilon$, $|S(t)|$ will be decreasing, until it reaches the set $\{|S| \leq \varepsilon\}$ in a finite time and remains inside thereafter. Inside the boundary layer where $|S| \leq \varepsilon$, we cannot have asymptotic stability and only uniformly ultimately bounded (UUB) stability with an ultimate bound can be obtained. The ultimate bound can be reduced by decreasing the depth of the boundary layer [22].

D. Controller Parameters Selection

According to the constraints of our experimental our VS system, the controller parameters are tuned to the selections shown in Table 1. First, based on the tradeoff between $\dot{e}$ and e from eq. (7) the rate of convergence (λ) is selected. Then from eq. (11), with respect to the maximum acceleration of the robot, and the maximum velocity of the goal object, function $\varphi(t)$ is chosen. According to the accuracy of the tracking error, β_0 is selected. The width of the boundary layer (ε) is tuned in order to reduce the oscillations of the control signal.

Table 1. THE CONTROLLER PARAMETERS

Type of switching function	φ	β_0	λ	ε
Signum	0.1	0.05	1	-
Saturation	0.1	0.13	1	$\varepsilon_x = \varepsilon_y = \varepsilon_z = 0.5$ $\varepsilon_A = \varepsilon_B = 0.38$

IV.   EXPERIMENTAL RESULTS

In this section, the performance of the proposed algorithm is verified through a few experiments. In the first experiment, efficiency of visual regulation with two different type of switching functions in SMC technique is performed. Second experiment verifies the overall performance of the servoing system.

A. Experiment I

Visual regulation is performed in this experiment. The pose of the end effector should be regulated accordingly for any arbitrary fixed pose of the object. The desired sliding mode manifold is produced based on the error between the estimated pose of the target with respect to the pose of the end effector. The main behavior of the control signal depends on the type of the switching function. Two different types of functions, signum and saturation, are employed. To analyze the behavior of these regulations, the initial pose of robot is reset to the same pose for each round of the experiment.

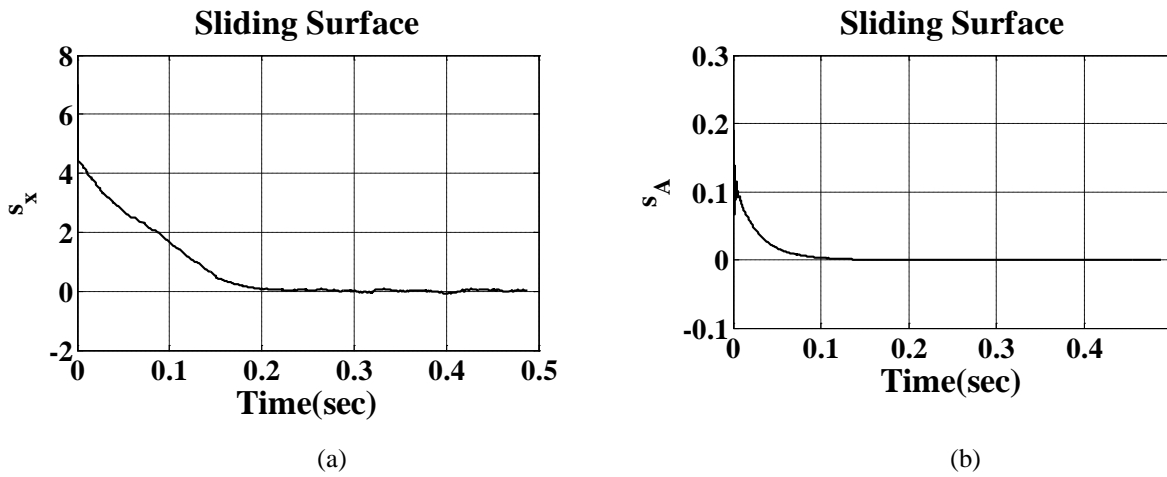(a)   (b)
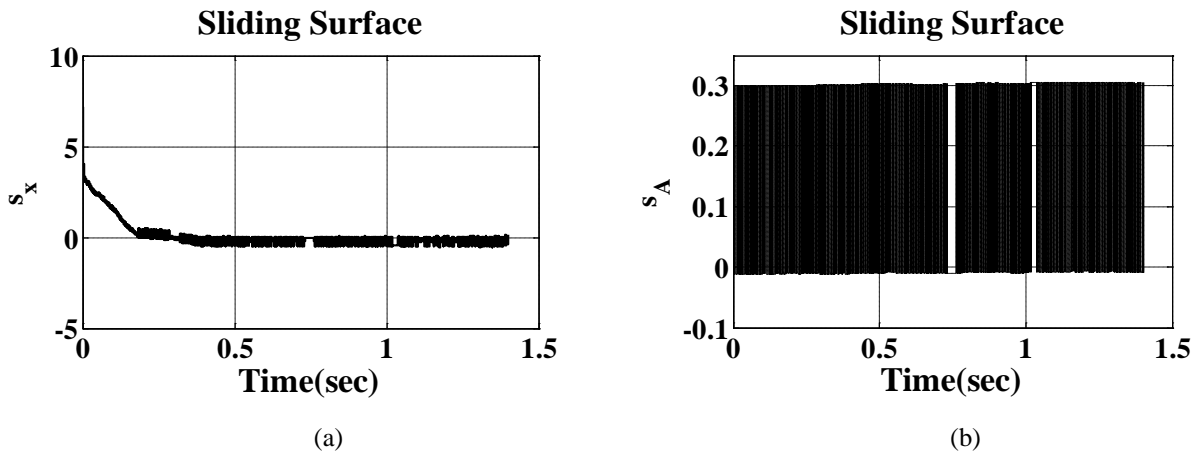
Fig. 5: Sliding surface with sign function in a: X direction, b: A orientation
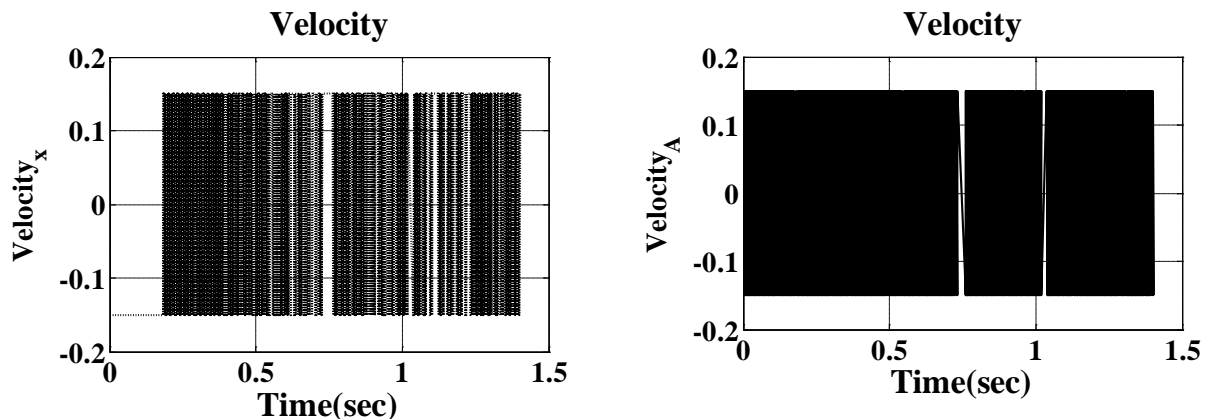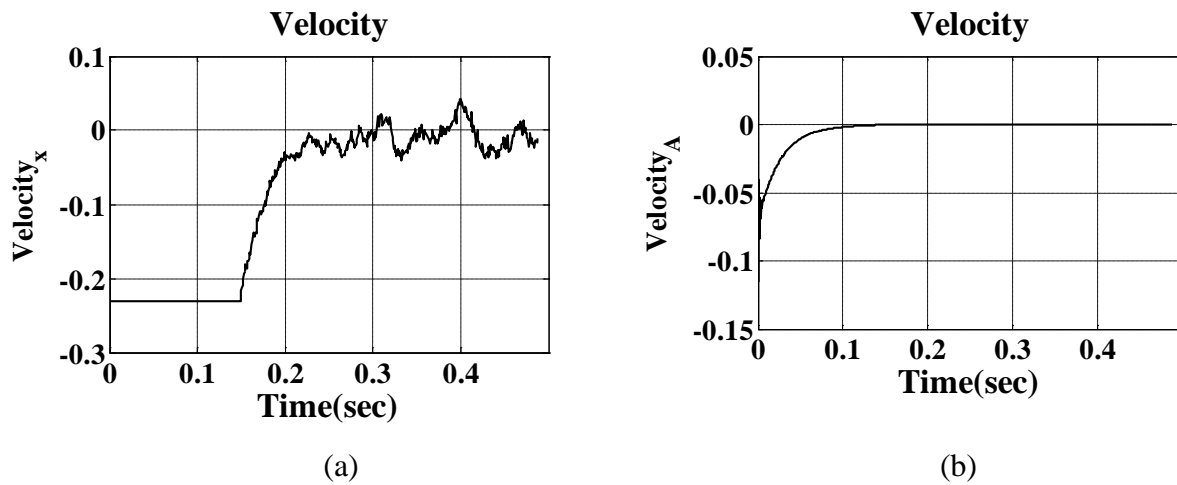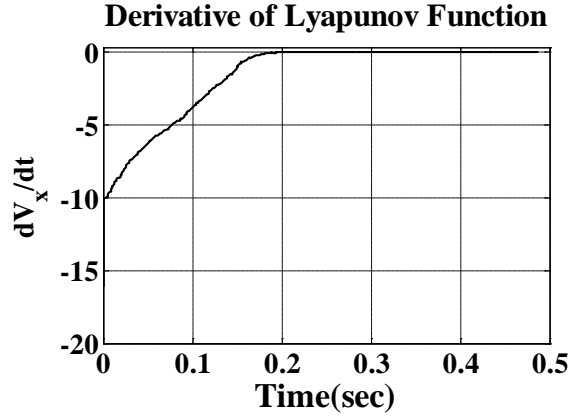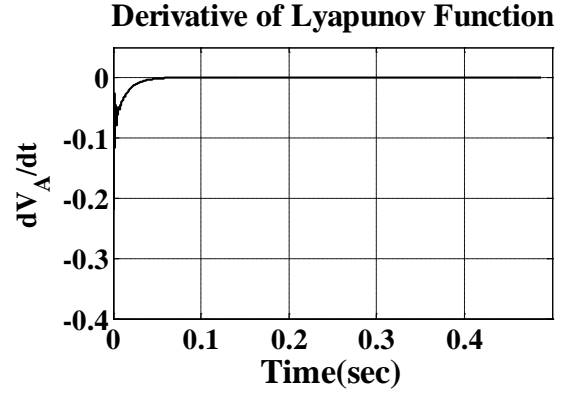
Fig. 6: Control signal with sign function in a: X direction, b: A orientation

Derivative of Lyapunov Function

Derivative of Lyapunov Function

(a)

(b)
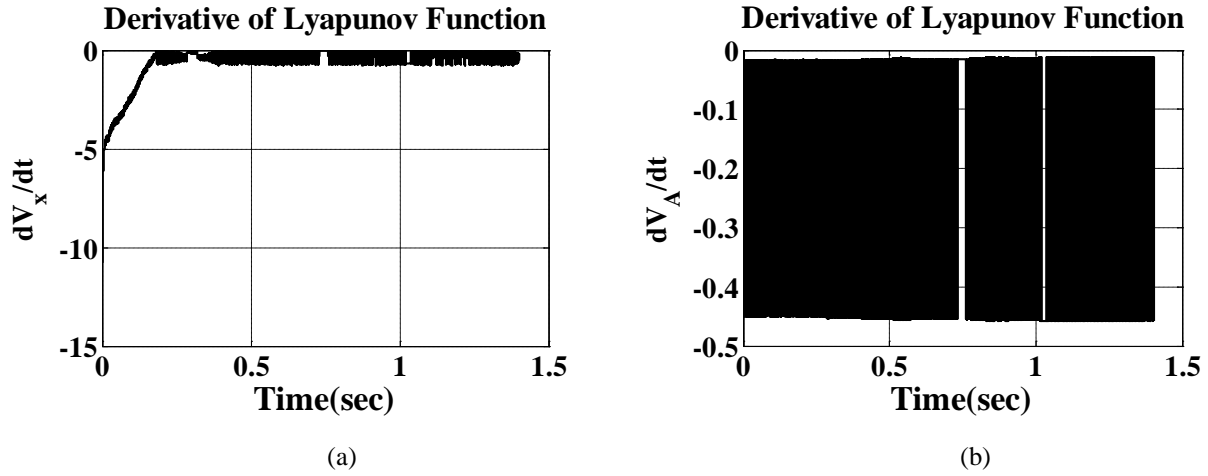
Fig. 7: Derivative of Lyapunov function with sign function in a: X direction, b: A orientation

The results of the sliding surface, the control signal (velocity signal) and the derivative of the Lyapunov function in the X direction and A orientation are shown in Fig. 5, Fig. 6 and Fig. 7 for signum function, respectively. The X direction and A orientation are selected as the representatives of translation and orientation respectively, to keep the number of illustrated figures at a managing level. As it can be seen in Fig. 5(part a), the trajectory lies on the sliding surface in the X direction and converges toward zero (in 0.2 second). The trajectories and the resulting sliding variables reach zero, which indicate that the error of the relative pose tend to zero in 0.8 second and lie on it after the object has been tracked. This issue can be seen in Fig. 6, too. The velocity in the X direction is produced as -0.15 cm per second during the first 0.2 second and after the tracking error tends to zero. The oscillations are due to the chattering; however, the variations remain around zero. This indicates that the controllers have suitably commanded the robot to stay on the sliding surface. As the object has no rotational motion, the control signal and the sliding surface in the A orientation are dithering around zero as Fig. 5 and Fig. 6 (part b). Fig. 7 shows that the derivative of the Lyapunov function is always negative which verifies the stability of this algorithm in practice.

In our case, the oscillations cannot significantly harm the mechanical parts of robot, since they are attenuated through the implemented filters in the inner structure of the robot. In practice, the chattering phenomenon is not desirable. To have a better performance in controlling the robot, we replaced the signum function by the saturation function. The results of this case for the sliding

surface, the control signal and the derivative of the Lyapunov function in the X direction and A orientation are shown in Fig. 8, Fig. 9 and Fig. 10 respectively. The trajectories and the resulting sliding variable reach the desired condition about 0.2 second, however, between 0.2 and 0.5 seconds the tracking errors are not exactly zero, and they are restricted in a bounded region. This is in the complete agreement of the stability analysis that guarantees only UUB condition on the tracking errors. In Fig. 9, the same behavior can be seen in the control signal, too. The signal is produced in the X direction as -0.22 cm per second and after that, this signal reaches zero in 0.15 second. This signal is not smooth, but the oscillations are significantly reduced. Since the object has no rotational motion, the control signal and the sliding surface are reached zero in 0.15 second. Fig. 10, illustrates the derivative of the Lyapunov function which is negative during the end effector movement. This verifies the overall stability of this algorithm.

(a) (b)

Fig. 8: Sliding surface with sat function in a: X direction, b: A orientation

(a) (b)

Fig. 9: Control signal with sat function in a: X direction, b: A orientation

(a)

(b)

Fig. 10: Derivative of Lyapunov function with sat function in a: X direction, b: A orientation

Table 2. THE Obtained relative position from UKO estimator

Position/Orientation	Initial Real Value	Initial Estimated Value	Final Estimated Value
X (cm)	9	9.03	0.25
Y (cm)	6.5	-6.59	-0.24
Z (cm)	28	27.78	18.10
A (deg)	-25	-23.91	1.00
B (deg)	0	2.02	0.81

(a)

(b)

Position

(c)

(d)

(e)

Fig. 11: UKO+KF estimation of motion in a: X direction, b: Y direction, c: Z direction, d: A orientation, e: B orientation

The results of regulating the robot pose from an initial relative pose to the desired position is numerically summarized in Table 2. The estimated values which are shown in Table 2 are from UKO+KF estimator. The "Initial Estimated Value" refers to the relative pose before the end effector movement. The "Final Estimated Value" denotes the relative pose after movement. Before performing experiment I, the "Initial Real Value" is set manually. By comparing the estimated and the real pose of the target object from this experiment and experiment II in [11], the nonlinear controller increases the performance of VS system (i.e. the "Final Estimated Value" for the pose of the object is close to the desired pose). The desired pose difference between the end effector and the target object is zero in the X, Y directions and A, B orientations, but the distance is 18cm in the Z direction (for safety). By assuming stop condition in our algorithm, we prevent the small movement of robot because of the measurement noise around the desired pose.

Thus, for the "Final Estimated Value", we will not have exactly zero. The numerical results signify the effectiveness of the suitable applied estimator in the visual regulation methodology.

B. Experiment II

The evaluation of the overall performance of the proposed visual servoing technique is the aim of experiment II, which is done through designing a few independent motions of the object. For this purpose, the object is moved in the X, Y, Z, A and B directions. According to the previous experiment, a saturation type SMC with the width of ε is considered for experiment II.

In order to comprehend the experiment better, the estimated relative pose of the target object with respect to the camera frame has been shown in the Fig. 11 for all directions, during the object movement. To show the tracking errors performance, Fig. 12, depicts the sliding mode surface only in the Y direction and B orientation as samples. Fig. 11 shows that when the object moves in any directions, the errors with respect to this motion will rapidly grow, and therefore, the corresponding sliding surface will grow. Then the proposed controller algorithm commands the end effector to move toward the target. For example, focus on the estimated relative poses in the X direction of Fig. 11 (part a) after about 6 seconds, the object started to move to approximately -6cm. Proportional to this movement the sliding surface in the X direction is generated, and the controller compensates these errors after approximately 4 seconds, which will decrease to zero. Similar analysis can be observed for B orientation, as well. Fig. 11 (part e) and Fig. 12 show that at 25 seconds the object starts to rotate around Y axis by about 22 degrees, the estimator detects this rotation. Consequently, the controller rotates the end effector and the errors decrease down to zero. The dash line shows the desired relative pose in each direction, that the robot manipulator is able to keep the desired relative distance. Table 3, shows the performance of the end effector movement, numerically.

Table 3. Performance of Tracking in Visual Servoing Experiment

Position/ Orientation	Initial Time of Movement (sec)	Time of Tracking (sec)	Compensated Relative Distance (cm)
X (cm)	6	10	-6.0
Y (cm)	10	14	+6.0
Z (cm)	16	19	-5.0
A (deg)	19	24	+16.89 & -27.75
B (deg)	25	30	22

Sliding Surface

Sliding Surface

(a)

(b)

Fig. 12: Sliding surface in a: Y direction, b: B orientation

Derivative of Lyapunov Function

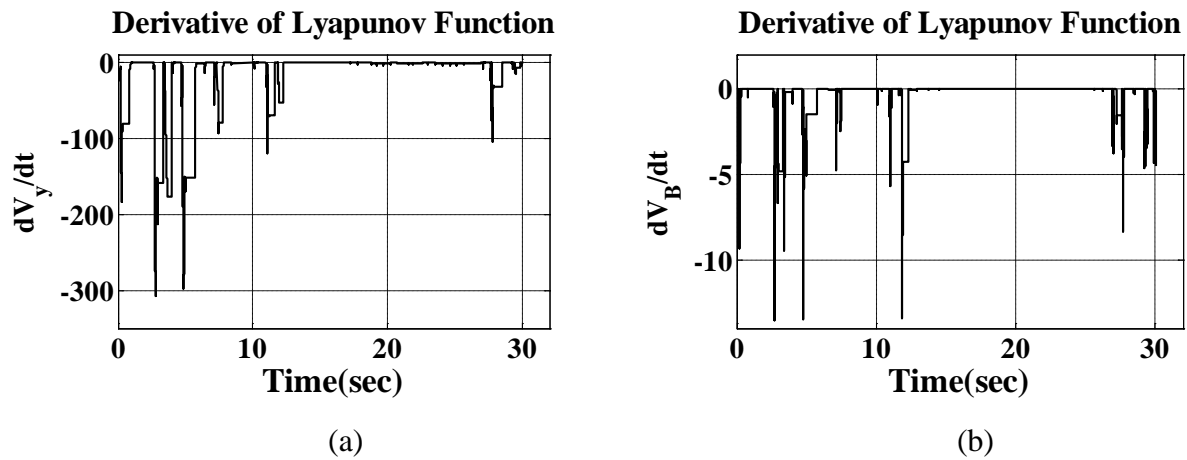**Derivative of Lyapunov Function**

(a)

(b)

Fig. 13: Derivative of Lyapunov function in a: Y direction, b: B orientation

To analyze the stability of visual servoing for the moving object, consider Fig. 13 that depicts the derivatives of the Lyapunov function which is a suitable measure for the proposed controller strategy. The sliding surfaces in Fig. 12 and the derivative of the Lyapunov functions in Fig. 13 show non smooth movement. At first glance, the jitters in the plots seem to be non smooth movement, but if the plot is suitably magnified at the vicinity of jitters, it can be seen that the signal is really smooth. This fact was shown in experiment I, and the performance is smooth and proper. Note that, as the target is moved by human, the recorded trajectory includes minute oscillations and vibrations which stems from the human hand motions. For the detail examination of the overall performance of the VS system a video clip is given in:

http://saba.kntu.ac.ir/eecd/aras/movies/SMC-Vservo.mpg.

V.   CONCLUSIONS

In this paper, we present a sliding mode controller in PBVS approach to control and path-plan an Industrial robot manipulator. By combining two mentioned tasks through SMC technique we can have a unified approach to tune the whole control system in all DOF of robot manipulator. In the proposed approach, the position, velocity and acceleration of the target object are estimated through a robust estimator (UKO+KF). The estimated values are applied to define a PD-type sliding mode surface. Then a stable and robust SMC is employed to produce a suitable control signal to move the robot toward the desired target. In order to select the controller parameters, we have considered some practical limitations and error bounds, which assume minimization of the relative pose in each DOF of the robot manipulator in hand. In experiments, we have observed that the proposed structure is performing well in a noisy background. It may be concluded that, this technique can be used for the industrial implementation of a visual servoing system. The idea of using SMC can be extended for IBVS approach. The stability analysis of this algorithm can be investigated under uncertainties, and as a result controller parameters can be tuned with specific objectives in future work.

REFERENCES

[1] Malis, E. and Benhimane, S. "A Unified Approach to Visual Tracking and Servoing", Robotics and Autonomous Systems, **52**(1), pp. 39-52 (2005).

[2] Gans, N. R. and Hutchinson, S. A. "Stable Visual Servoing through Hybrid Switched-System Control", IEEE Trans. on Robotics, **23**(3), pp. 530-540 (2007).

[3] Hutchinson, S. and Hager, G. D. and Croke, P. I. "A Tutorial on Visual Servo Control", IEEE Trans. on Robotics and Automation, **12**(5), pp. 651-670 (1996).

[4] Chesi, G. and Vicino, A. "Visual Servoing for Large Camera Displacements", IEEE Trans. on Robotics, **20**(4) pp. 724-735 (2004).

[5] Chaumette, F. and Hutchinson, S. "Visual Servo Control Part I: Basic Approaches", IEEE Robotics and Automation Magazine, **13**(4), pp. 82-90 (2006).

[6] Malis, E. and Mezouar, Y. and Rives, P. "Robustness of Image Based Visual Servoing with a Calibrated Camera in the Presence of Uncertainties in the Three-Dimensional Structure", IEEE Trans. on Robotics, **26**(1), pp. 112-120 (2010).

[7] Malis, E. and Chaumette, F. and Boudet, S. "2 1/2–D Visual servoing", IEEE Trans. Robot. Automat., **15**, pp. 238-250 (1999).

[8] Wilson, W. J. "Relative end effector control using Cartesian position based visual servoing", IEEE Trans. on Robotics and Automation, **12**(5), pp. 684-696 (1996).

[9] Taghirad, H. D. and Atashzar, S. F. and Shahbazi, M. " A Robust Solution to Three-Dimensional Pose Estimation Using Composite Extended Kalman Observer and Kalman Filter", IET Computer Vision, **6**(2), pp. 140-152 (2012).

[10] Janabi-Sharifi, F. and Marey, M. "A Kalman-Filter- Based Method for Pose Estimation in Visual Servoing", IEEE Trans. on Robotics, **26**(5), pp. 939-947 (2010).

[11] Salehian, M. and RayatDoost, S. and Taghirad, H. D. "Robust Unscented Kalman Filter for Visual Servoing System", the 2nd International Conference on Control, Instrumentation, and Automation (ICCIA), Shiraz, Iran, pp. 1006-1011 (2011).

[12] Stepanenko, Y. and Cao, Y. and Su, C. Y. "Variable Structure Control of Robotic Manipulator with PID Sliding Surfaces", International Journal of Robust and Nonlinear Control, **8**(1), pp. 79-90 (1998).

[13] Zanee, P. and Morel, G. and Plestan, F. "Robust Vision Based 3D Trajectory Tracking Using Sliding Mode Control", Proc. of the IEEE Int. Conf. on Robotics and Automation, **3**, pp. 2088-2093 (2000).

[14] Kim, J. K. and Kim, D. W. and Choi, S. J. and Won, S. C. "Image-based Visual Servoing using Sliding Mode Control", SICE-ICASE International Joint Conference, pp. 4996-5001 (2006).

[15] Zanee, P. and Morel, G. and Plestan, F. "Robust 3D Vision Based Control and Planning", Proc. of the IEEE Int. Conf. on Robotics and Automation, **5**, pp. 4423-4428 (2004).

[16] Li, F. and Xie, H. L. "Sliding Mode Variable Structure Control for Visual Servoing System", International Journal of Automation and Computing, **7**(3), pp. 317-323 (2010).

[17] Sim, T. P. and Hong, G. S. and Lim, K. B. "Modified Smith Predictor with DeMenthon-Horaud pose estimation algorithm for 3D dynamic visual servoing", Robotica, **20**(6), pp. 615–624 (2002).

[18] Yoon, Y. and Kosaka, A. and Kak, A. C. "A New Kalman- Filter-Based Framework for Fast and Accurate Visual Tracking of Rigid Objects", IEEE Trans. on Robotics, **24**(5), pp. 1238- 1251 (2008).

[19] Wang, J. H. and Chen, J. B. "Adaptive Unscented Kalman filter for initial alignment of strapdown inertial navigation systems", Proc. of the Ninth Int. Conf. on Machine Learning and Cybernetics, Qingdao, **3**, pp. 1384-1389 (2010).

[20] Taghirad, H. D. and Shahbazi, M. and Atashzar, S. F. and RayatDoost, S. "A Robust Pose-Based Visual Servoing Technique for Redundant Manipulators", submitted to Robotica, (2012).

[21] Eric A. Wan and Rudolph van der Merwe, "The Unscented Kalman Filter for Nonlinear Estimation", in Proc. of IEEE Symposium 2000 (AS-SPCC), Lake Louise, Alberta, Canada, Oct, pp. 153-158 (2000).

[22] Slotine, J. E. "Sliding Controller Design for Nonlinear Systems", Int. Journal of Control, **40**(2), pp. 421-434 (1984).

[23] Khalil, H. K. "Nonlinear Systems", 3rd edition, Prentice Hall, Upper Saddle River, New Jersey, (2005).

Mahsa Parsapour received her B.Sc. and M.Sc. degrees in electrical engineering from K.N. Toosi University of Technology, Tehran, Iran, in 2011 and 2013, respectively. She is currently a researcher at the Advanced Robotics and Automated System (ARAS) group at K.N. Toosi University of Technology, Tehran, Iran. Her research work is in robotics, visual servoing, nonlinear control, and image processing.

Soheil RayatDoost received his B.Sc. degree in electrical engineering from K.N. Toosi University of Technology, Tehran, Iran, in 2009. After that, he worked as a researcher at the Advanced Robotics and Automated System (ARAS) group at K.N. Toosi University of Technology until 2013. He received M.Sc. degree from department of electrical and computer engineering, University of Tehran, Iran, in 2014. His current research interests include: Pattern Recognition, Computer Vision, Affective Computing, Identification and Robotics.

Hamid D. Taghirad received his B.Sc. degree in mechanical engineering from Sharif University of Technology, Tehran, Iran, in 1989, his M.Sc. in mechanical engineering in 1993, and his Ph.D. in electrical engineering in 1997, both from McGill University, Montreal, Canada. He is currently a Professor and the dean of the Faculty of Electrical Engineering, and the Director of the Advanced Robotics and Automated System (ARAS) at K.N. Toosi University of Technology, Tehran, Iran. He is a senior member of IEEE, the chairman of IEEE control system chapter in Iran section member of the board of Industrial Control Center of Excellence (ICCE), at K.N. Toosi University of Technology, editor in chief of Mechatronics Magazine, and Editorial board of International Journal of Robotics: Theory and Application, and International Journal of Advanced Robotic Systems. His research interest is robust and nonlinear control applied to robotic systems His publications include five books, and more than 190 papers in international Journals and conference proceedings.

List of the Figure Captions
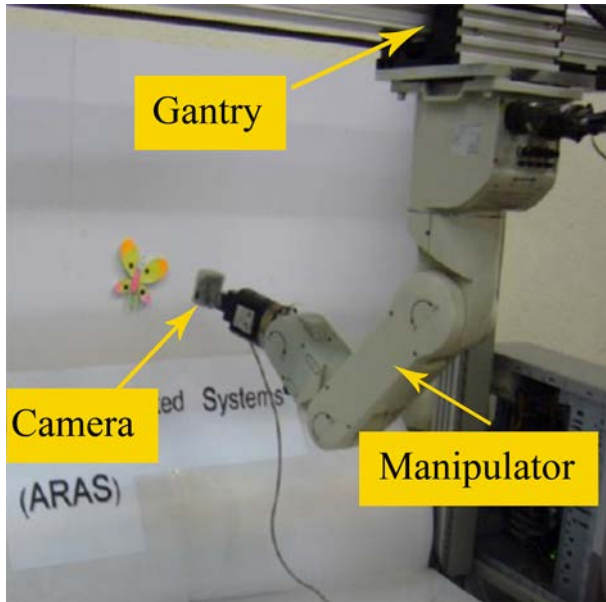
Fig. 1: Experimental setup

Name of Figure: Fig1.eps
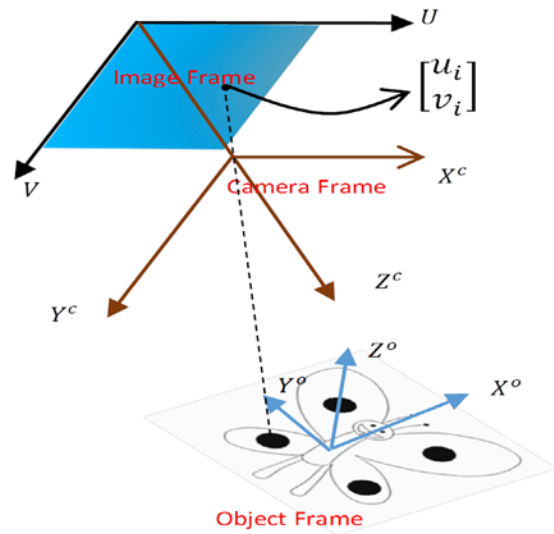
Fig. 2: Camera, object and image frames

Name of Figure: Fig2.eps
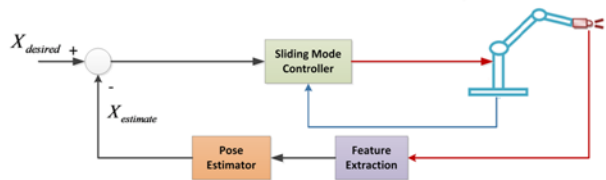
Fig. 3: The complete VS loop

Name of Figure: Fig3.eps
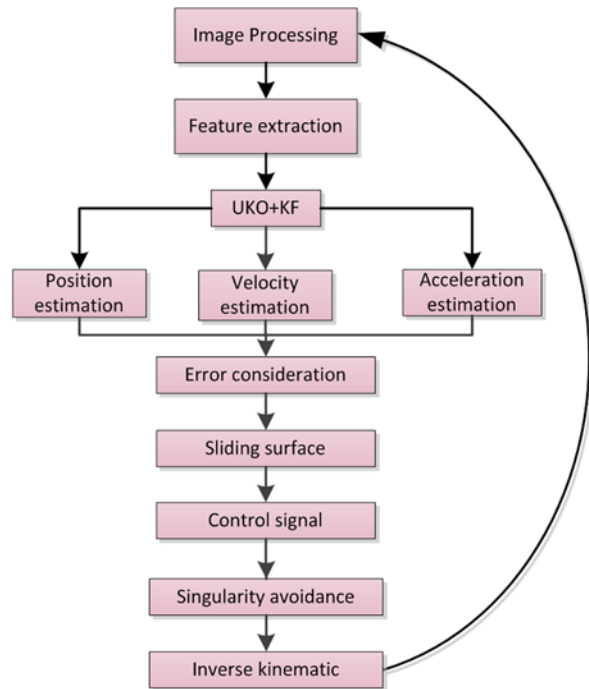
Fig. 4: Block diagram of the overall process

Name of Figure: Fig4.eps
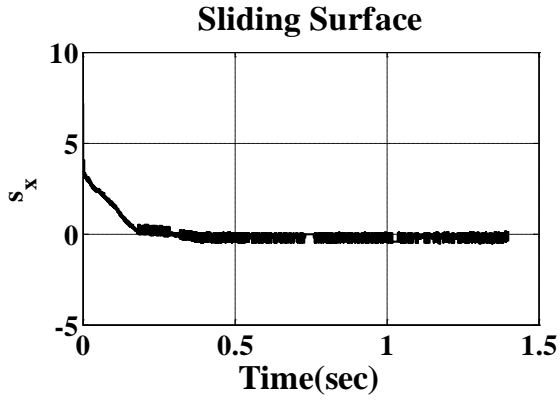
Sliding Surface

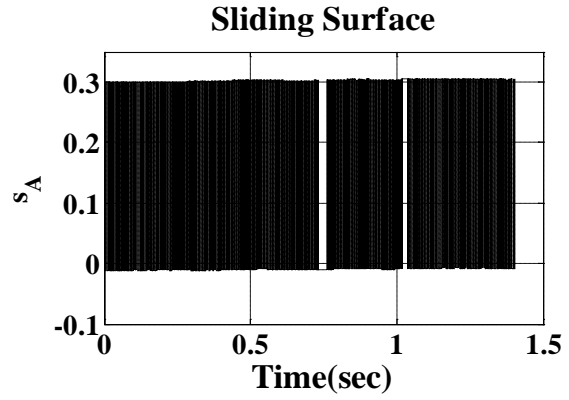

Fig. 5(a): Sliding surface in X direction

Name of Figure: Fig5-a.eps

Sliding Surface

Fig. 5 (b): Sliding surface in A direction
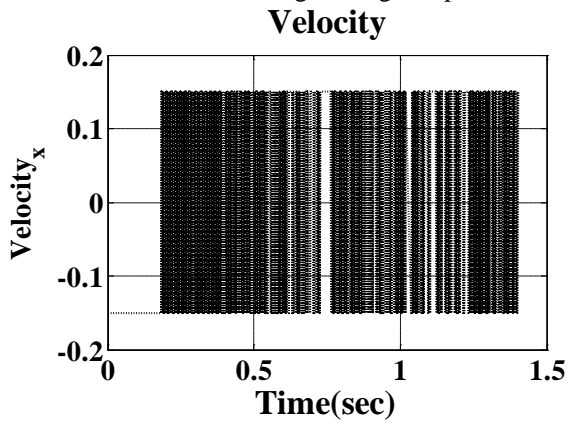
Name of Figure: Fig5-b.eps

Velocity

Fig. 6(a): Control signal in X direction

Name of Figure: Fig6-a.eps

Velocity
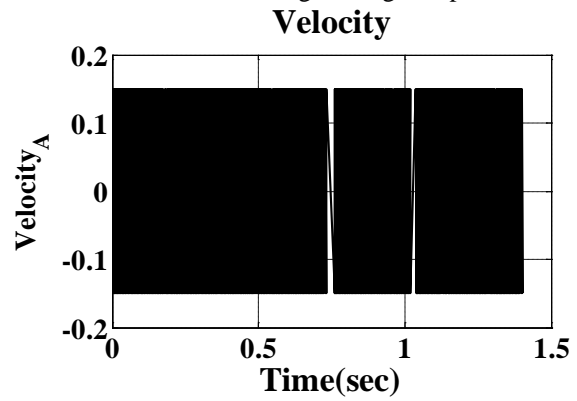
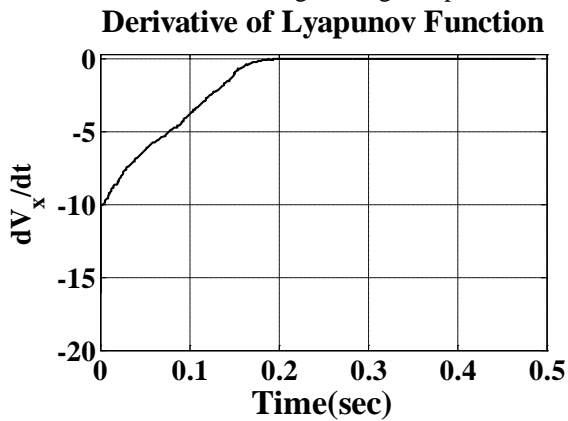Fig. 6(b): Control signal in A direction

Name of Figure: Fig6-b.eps

Derivative of Lyapunov Function
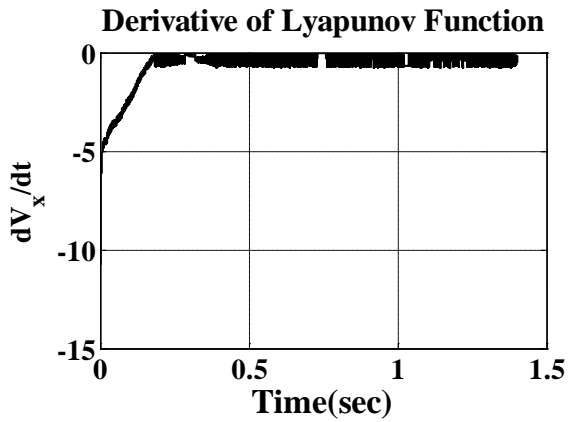
Fig. 7(a): Derivative of Lyapunov function in X

direction

Name of Figure: Fig7-a.eps

Derivative of Lyapunov Function
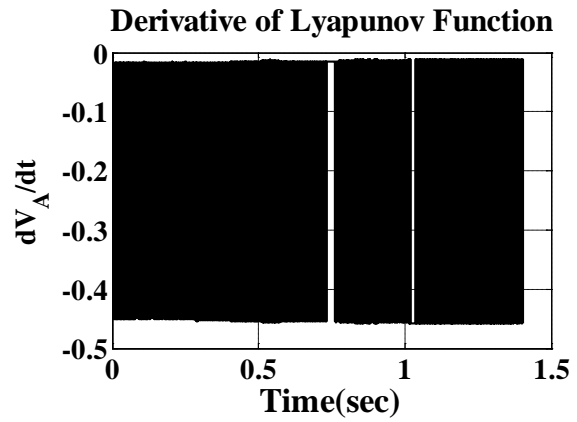
Fig. 7(b): Derivative of Lyapunov function in A

direction

Name of Figure: Fig7-b.eps
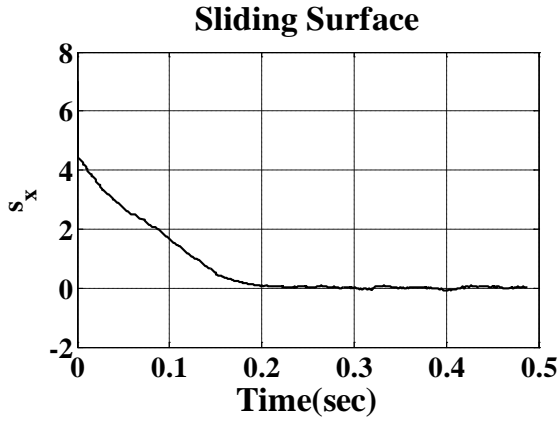
Sliding Surface

Fig. 8(a): Sliding surface in X direction

Name of Figure: Fig8-a.eps
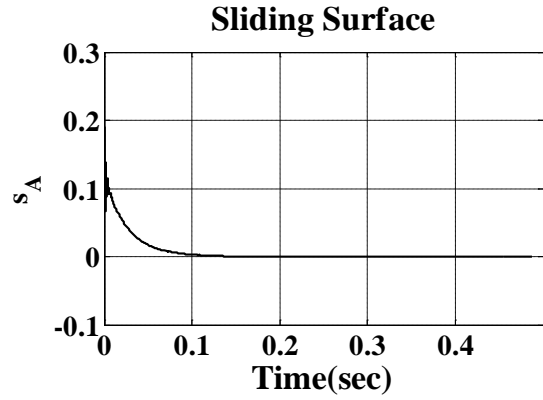
Sliding Surface

Fig. 8(b): Sliding surface in A direction

Name of Figure: Fig8-b.eps

Velocity
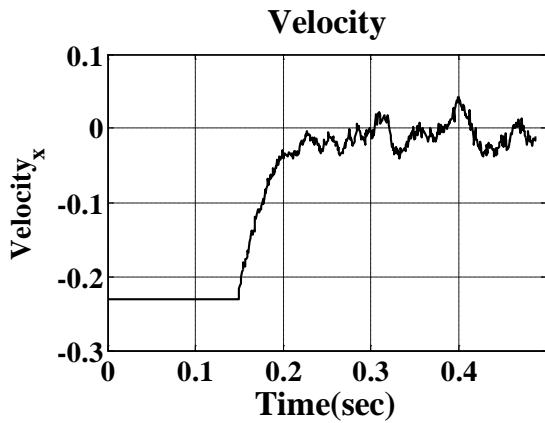
Fig. 9(a): Control signal in X direction

Name of Figure: Fig9-a.eps

Velocity
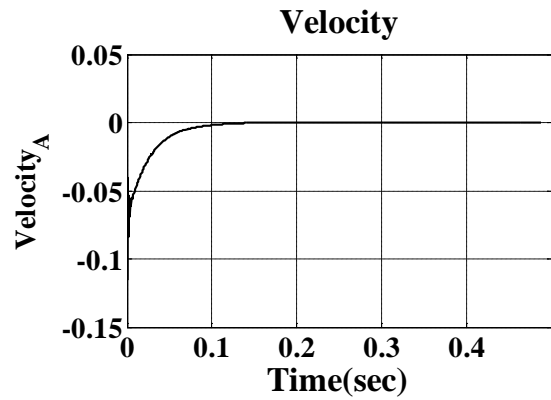
Fig. 9(b): Control signal in A direction

Name of Figure: Fig9-b.eps

Derivative of Lyapunov Function

Fig. 10(a): Derivative of Lyapunov function in X direction

Name of Figure: Fig10-a.eps

Derivative of Lyapunov Function
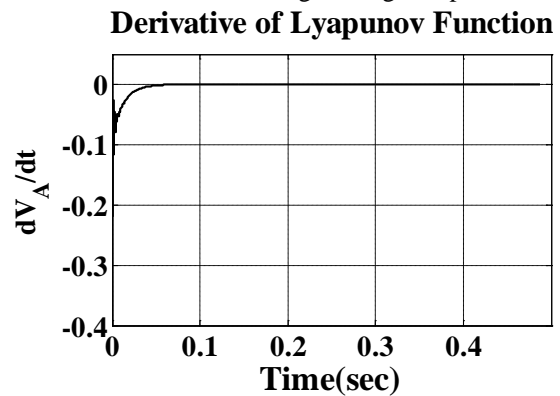
Fig. 10(b): Derivative of Lyapunov function in A direction

Name of Figure: Fig10-b.eps
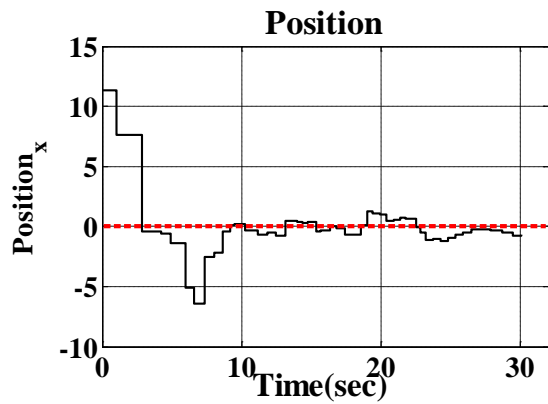
Fig. 11 (a): Estimated Pose in X direction

Name of Figure: Fig11-a.eps
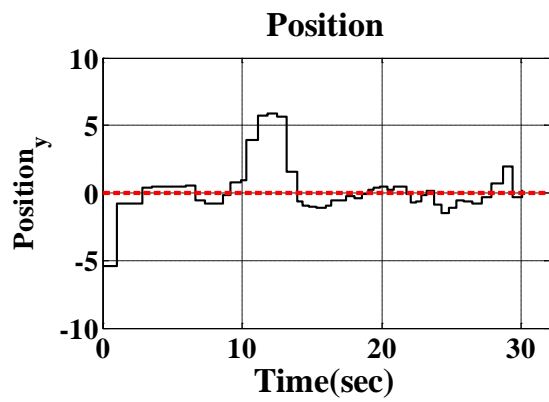
Fig. 11 (b): Estimated Pose in Y direction

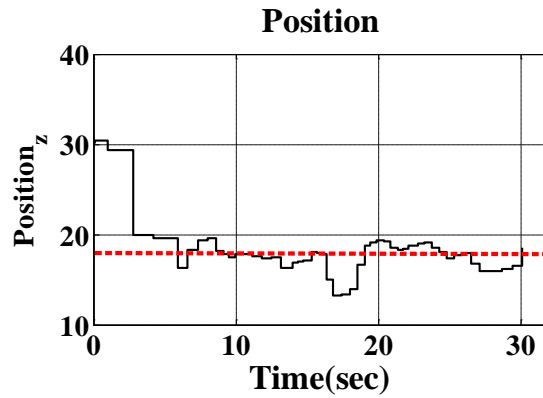Name of Figure: Fig11-b.eps

Fig. 11 (c): Estimated Pose in Z direction
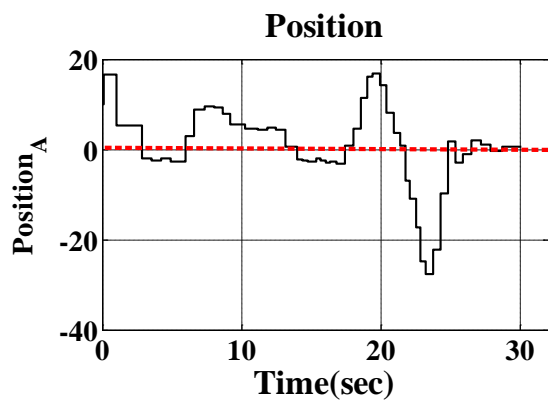
Name of Figure: Fig11-c.eps

Fig. 11(d): Estimated Pose in A direction
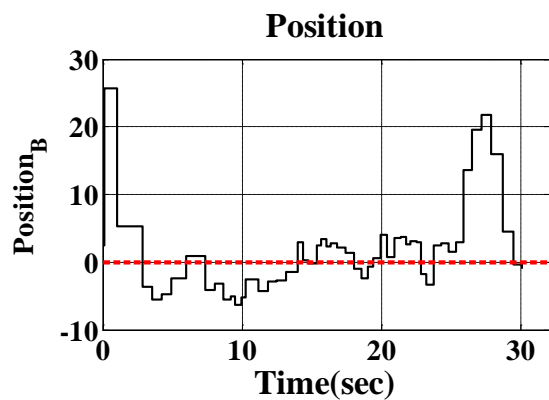
Name of Figure: Fig11-d.eps

Fig. 11(e): Estimated Pose in B direction
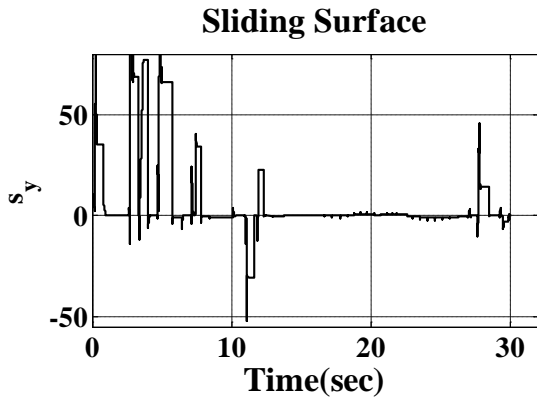
Name of Figure: Fig11-e.eps

Sliding Surface

Fig. 12(a): Sliding surface in Y direction

Name of Figure: Fig12-a.eps
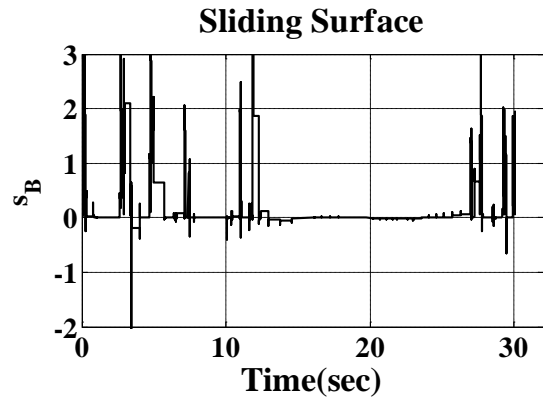
Sliding Surface

Fig. 12(b): Sliding surface in B direction

Name of Figure: Fig12-b.eps

Derivative of Lyapunov Function
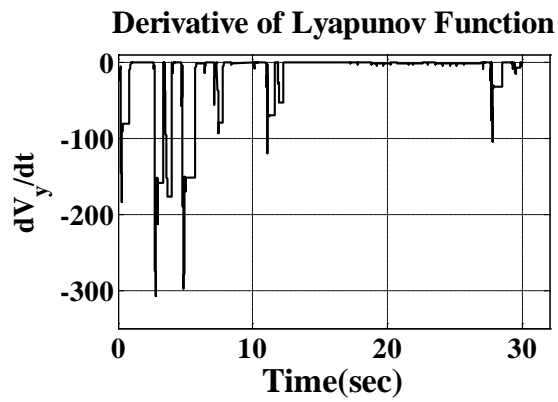

Fig. 13(a): Derivative of Lyapunov function in Y

direction

Name of Figure: Fig13-a.eps
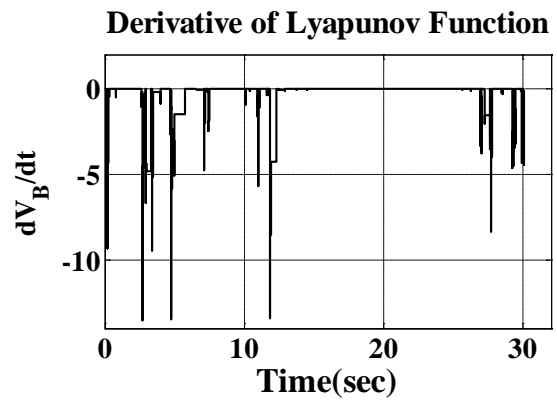
Derivative of Lyapunov Function

Fig. 13(b): Derivative of Lyapunov function in B

direction

Name of Figure: Fig13-b.eps

List of the Table Captions

TABLE 1. THE CONTROLLER PARAMETERS

Type of switching function	φ	β_0	λ	ε
Signum	0.1	0.05	1	-
Saturation	0.1	0.13	1	$\varepsilon_x = \varepsilon_y = \varepsilon_z = 0.5$ $\varepsilon_A = \varepsilon_B = 0.38$

TABLE 2. THE OBTAINED RELATIVE POSITION FROM UKO ESTIMATOR

Position/ Orientation	Initial Real Value	Initial Estimated Value	Final Estimated Value
X (cm)	9	9.03	0.25
Y (cm)	6.5	-6.59	-0.24
Z (cm)	28	27.78	18.10
A (deg)	-25	-23.91	1.00
B (deg)	0	2.02	0.81

TABLE 3. PERFORMANCE OF TRACKING IN VISUAL SERVOING EXPERIMENT

Position/ Orientation	Initial Time of Movement (sec)	Time of Tracking (sec)	Compensated Relative Distance (cm)
X (cm)	6	10	-6.0
Y (cm)	10	14	+6.0
Z (cm)	16	19	-5.0
A (deg)	19	24	+16.89 & -27.75
B (deg)	25	30	22